FACTA UNIVERSITATIS
Series: **Electronics and Energetics** Vol. 39, Nº 1, March 2026, pp. 13 - 40
https://doi.org/10.2298/FUEE2601013H

Original scientific paper

PERFORMANCE ANALYSIS OF LEAD ACID BATTERY HEALTH USING KALMAN RESIDUALS THROUGH THE DEVELOPMENT OF SMART MONITORING SYSTEM FOR ELECTRIC THREE-WHEELERS

Suman Haldar[1], Arindam Mondal[2], Rajib Banerjee[3]

[1]NITMAS, Department of Electronics and Communication Engineering, India
[2]BCREC, Department of Electrical Engineering, India
[3]UPES, Department of Computer Science, India

ORCID iDs:	Suman Haldar	https://orcid.org/0000-0002-7073-323X
	Arindam Mondal	https://orcid.org/0000-0003-3210-1685
	Rajib Banerjee	https://orcid.org/0000-0003-0685-5977

Abstract. *Monitoring battery health is an important aspect of accurately predicting the operational lifespan of batteries in electric vehicles. The battery terminal voltage, current, and temperature are the primary factors influencing battery durability and determine how long it will last before failure occurs. For commercially viable Electric Three Wheeler (E3W), an economical yet highly precise data acquisition system (DAQ) is crucial. Currently, commercially available lead-acid (PbA) battery-powered E3Ws lack a dedicated DAQ for the continuous monitoring of battery performance. In this research we develop "SMDAQ" a smart multichannel DAQ to address this gap, enabling real-time monitoring of these critical parameters. The system is specifically designed for the PbA batteries commonly used in E3Ws. The prototype uses a noninvasive, dual-polarity-based current sensing technology to distinguish between charging and discharging cycles, detecting high current discharges up to 60A. It also incorporates custom temperature sensor probes capable of measuring temperatures up to 60℃ in multiplexed mode. The system records terminal voltage up to 16.5V and traction battery pack voltage up to 66V using the node voltage subtraction method for accurate monitoring. Integrated with a data transmission and backup mechanism, the SMDAQ system stores data locally in flash memory and remotely on the cloud, offering user-friendly queries for battery parameters. It features discharge analysis and State of Health (SOH) assessment using a data-driven Root Mean Square Error (RMSE) and Kalman Filter Residual approach under varying discharge conditions. Battery anomalies are analyzed under different C-rate and depth of discharges. With 98.6% accuracy, prototypes have been tested for over 1000 hours, ensuring reliable performance.*

Key words: *Data acquisition system, battery monitoring system, state of health, microcontroller, electric three-wheeler.*

Received February 24, 2025; revised April 24, 2025 and May 15, 2025; accepted May 16, 2025
Corresponding author: Arindam Mondal
Department of Electrical Engineering, Dr. B.C Roy Engineering College, Durgapur-713206,India
E-mail: arininstru@gmail.com

1. INTRODUCTION

In response to environmental and energy challenges, battery-operated vehicles (BOVs) have emerged as a sustainable alternative to internal combustion engine (ICE) vehicles, offering zero emissions, lower operating costs, and up to 77% overall efficiency compared to ICE counterparts [1][2][3]. The E3W market in the Asia-Pacific region is projected to reach 702.1 thousand units by 2027, with a CAGR exceeding 20%, driven by lower maintenance costs and increased adoption for last-mile transport and logistics, especially in rural and suburban areas [4]. E3Ws predominantly use lead-acid (PbA) and lithium-ion batteries (LIB), with PbA favored due to its low cost, proven reliability, and specific power range of 75–200 W/kg. The advanced PbA variants like VRLA gel and AGM have improved performance and offer maintenance-free solutions [5], playing a crucial role in the operational efficiency and affordability of E3Ws in suburban and rural areas of the Asia Pacific region [6].Therefore, significant advancements are still needed for BOVs to reach the efficiency and affordability of traditional ICE vehicles. Extending battery longevity plays a crucial role in reducing overall running expenses. As a result, researchers are dedicated to designing better battery monitoring and management systems to maximize battery life [7]. Accurate monitoring of battery health, including Remaining Useful Life (RUL), is essential for predictive maintenance and efficient operation [8][9].Onboard batteries of BOVs experience electrical stress during operation due to inconsistent current demands, which can lead to issues such as deep discharge and the need for frequent battery replacements [10]. However, this excessive discharging may lead to transient short circuits, which ultimately reduce the load terminal voltage and consequently the battery capacity [11]. Additionally, thermal effects from overcharging can accelerate chemical degradation, adversely affecting State of Health (SOH) [12][13]. In this context, an exact measurement and effective battery parameters monitoring system are crucial to predict the lifespan of on board vehicle batteries. To address the battery behavior throughout its charging and discharging cycle, a real-time monitoring system is more relevant for continuously tracking and recording key parameters such as voltage, current, and temperature. Simultaneously, it alerts vehicle operators based on pre assigned battery data markers ensuring timely intervention, safety compliance, reducing operational costs, and addressing intermittent battery issues.

This paper presents the design and development of IoT based Smart Multichannel Data Acquisition System (SMDAQ). This cost-effective highly accurate device measures and monitors critical parameters of the onboard PbA battery pack used as a main power source for E3W vehicles. In addition to its primary function, SMDAQ serves as a data-driven performance forecasting tool and offers crucial findings for both E3W owners and manufacturers to diagnose battery-related issues and optimize battery performance.

1.1. Literature Survey

Battery life plays a vital role in the overall cost of operating BOVs, as frequent replacements remain one of the major expenses. To manage battery degradation, the State of Health (SOH) is used, calculated as the ratio between current and initial maximum capacity in ampere-hours, while the State of Charge (SOC) indicates the available capacity at any moment [14]. These parameters are essential in influencing a vehicle's performance, range, charging efficiency, and safety [15][16]. Lead-acid (PbA) batteries continue to dominate the rechargeable battery market, accounting for over 70% of global sales, due to their affordability and mature technology. As battery health directly impacts vehicle

reliability, various SOH estimation techniques have been explored, including model-based, direct measurement, and data-driven approaches to prevent failure and enhance predictive maintenance [17]. A critical extension of SOH evaluation is the estimation of Remaining Useful Life (RUL), which helps in optimizing charge-discharge cycles and extending operational lifespan [18]. To improve prediction accuracy, recent studies have increasingly adopted artificial intelligence techniques for RUL estimation, integrating big data, AI, and IoT for more dynamic and diverse assessment frameworks and physics-informed approaches [19]–[23]. In fact, study focuses on direct measurement and model-based methodologies, where SOH estimation is primarily conducted using battery capacity, power, internal resistance, and key performance indicators like voltage, current, and temperature [24]. Advances in deep neural networks (DNNs) have enabled statistical models for SOH and RUL estimation, with long short-term memory (LSTM) networks achieving RUL accuracy within ±10 cycles [25]. Temporal Convolutional Networks (TCNs) have also been introduced for SOH and RUL monitoring, using causal and dilated convolutions to enhance performance [26]. Battery performance parameters such as voltage and current are closely tied to internal resistance and load demand. Sudden voltage drops during current spikes indicate aging and degradation trends, while current fluctuations help identify overloading and usage anomalies [27]. Electrolyte temperature is another critical factor affecting SOH, as excessive heat from overcharging or high operating loads can accelerate chemical breakdown and reduce efficiency [28][29]. Numerous battery monitoring systems have been proposed to address these challenges. For instance, one study implemented a GSM-based BMS for a 12.8V, 10Ah $LiFePO_4$ battery, enabling remote transmission of key parameters [30]. Another system used ESP8266 and the ThingSpeak cloud to monitor a 28Ah lithium-ion battery in an electric two-wheeler application [31]. A more complex setup employed Raspberry Pi, ESP8266, and Arduino for low-current monitoring on a 26Ah PbA battery, though limited by cost and the absence of transient current detection [32]. Hybrid approaches combining machine learning and sensing technologies have also emerged. One lab-based DAQ system integrated with a thermistor, IRLZ44N MOSFET, CD74HC4067 multiplexer, ATMEGA 328 microcontroller, and ESP8266 WiFi was used to monitor lithium-ion battery voltage and temperature with overvoltage protection features, though it lacked capabilities for transient current measurement and detailed discharge trend analysis [33]. Similarly, a real-time IoT-based solution was proposed for high-capacity PbA batteries above 65Ah, but it was unsuitable for smaller-capacity applications [34]. Another study incorporated LoRa communication and ML to predict RUL in 1400mAh Li-ion batteries with high accuracy, yet lacked real-world testing under high-discharge cycles [35].Real-time DAQ systems are increasingly important for BOVs to track SOC, SOH, and thermal states, enabling predictive maintenance, fault detection, and analysis of usage patterns. One such system designed for E3Ws employed ESP32, ACS712, and LM35 sensors to measure discharge up to 30A but did not account for transient spikes or the impact of driving cycles [36]. Moreover, IoT-enabled platforms with GPS, GPRS, and motion sensors integrated via OBD-II ports have been proposed to assess vehicle behavior, route efficiency, and fleet performance [37][38]. Lastly, a critical gap remains between laboratory testing and real-world battery performance. A study emphasized the need for long-term experimental testing by analyzing field data collected over a year, revealing how driving behaviors, braking, acceleration, and ambient conditions influence SOH estimation and battery lifespan [39].

1.2. Research Gap and Contribution

Most existing battery monitoring systems rely on laboratory-based methods such as simulation and modeling. These approaches measure nominal voltage, current, and temperature under controlled environments for lithium-ion (Li-ion) and lead-acid (PbA) batteries. However, real-world conditions introduce complexities that lab-based methods fail to address, such as varying discharge rates (C rate), partial charging and discharging, and extended rest periods. These inconsistencies make it challenging to accurately determine the state of health (SOH) and state of charge (SOC) using direct measurement techniques or machine learning models, which require high-quality real-world data for precise predictions.

The key contributions are as follows:

- The development of the SMDAQ system enables the monitoring of individual terminal voltages (16.5V), pack voltage (66V), current (60A), and temperature (60°C) for comprehensive battery diagnostics.
- Data Backup and Retransmission (DBR) feature combined with a customized web application for real-time visualization and interpretation of field data.
- Analysis of DOD and C-rate discharging behavior for real-time performance evaluation.
- A dual-method SOH estimation framework combining RMSE and Kalman filter residual analysis for accurate battery health assessment.

The paper is organized as follows: section 2 outlines the system design and hardware architecture. software architecture and system operation are detailed in section 3 results and discussion are presented in section 4, followed by the conclusion in section 5.

2. System Design and Hardware Architecture for the Measurement of SoH Of Lead-Acid Batteries

SMDAQ is a portable battery parameter monitoring device featuring multiple analog input channels. These input channels are primarily intended for real-time data capturing and monitoring of onboard battery terminal voltage, current, and temperature at various drive cycles of E3W. The functioning and design of SMDAQ hardware circuits allow for the measurement and monitoring of a variety of battery parameters in a wide-span measurement without significantly modifying the hardware circuit. This is achieved by its customized program code, which guarantees operational versatility. The specifications of SMDAQ are illustrated in Table 1.

SMDAQ is an energy-efficient monitoring device consuming only 550 mW of power. The prototype measures voltage up to 66V at the pack level and 16.5V at the node level. This range is aligned with the PbA batteries during the bulk and absorption phase of the charging process. It supports the current range of up to 100A with an operation range of 50–60A during discharge of the E3W battery under different drive cycles. Additionally, custom-made temperature sensing probes are designed to monitor the battery's electrolyte temperature up to 60°C during both charging and discharging cycles. It offers measurement accuracy of ±2% (voltage), ±1.4% (current), and ±2°C (temperature). Data is logged at 130kB/hr with a recording frequency of up to 0.5 Hz and stored via microSD with DS3231 RTC for backup and retransmission. Therefore, SMDAQ provides a comprehensive battery monitoring solution that enhances energy optimization, contributing to improved performance and extended battery life of E3W.

Table 1 Specifications of SMDAQ

Specifications	Details	Specifications	Details
Power Consumptions	550 mW (for continuous operation)	Current Measurement Range	Up to 100 A with dual polarity indication (+ for discharging, - for charging)
Power Supply	5V DC (powered via E3W onboard battery)	Temperature Range	0°C to 60°C (battery electrolyte temperature monitoring)
Operating Conditions	Suitable for various E3W drive cycles	Accuracy	±2% (voltage), ±1.4 % (current), ±2°C (temperature)
Data Recording Rate	130kB/Hr and configurable up to 0.5 Hz (data recorded and updated every 2- second)	Communication Interfaces	SPI/I2C/TWI/USB and Web-based GUI for real-time visualization and interpretation of data
Data Backup and Retransmission (DBR)	Integrated micro SD storage with DS3231RTC module for data backup and retransmission with third-party data server	Sensor Type	WCS 1600 current sensor, four-channel temperature sensing probes, resistive divider network
Input voltage Range	0-16.5V (individual battery) and up to 66V (pack level)	Connectivity Protocol	IEEE802.11

2.1. System Level Description

Figure 1 shows the system-level block diagram of the SMDAQ DAQ. The architecture includes seven key components: battery voltage sensing, current sensing, temperature probes, memory and real-time clock (RTC) interface, signal multiplexing and conditioning, microcontrollers, and a cloud-based monitoring interface. The core of the system is an ATmega328P 8-bit microcontroller, which manages all sensing operations. Battery voltages are monitored using a four-channel sensor network with low-pass filters and diode protection. Charging/discharging current is measured using a non-invasive sensor followed by a second-order low-pass filter for noise reduction. Custom temperature probes interface with a conditioning circuit for accurate thermal monitoring. An analog multiplexer handles multiple inputs (voltage, current, temperature), minimizing the need for multiple ADCs and reducing system complexity and cost. Wireless data transmission and cloud integration are handled by an ESP8266 microcontroller, which communicates with the ATmega328P via UART and connects to the internet over IEEE 802.11. The system also features onboard memory and RTC for data backup and time stamping. Real-time data is visualized through a user-specific cloud interface, ensuring reliable and continuous battery health monitoring.

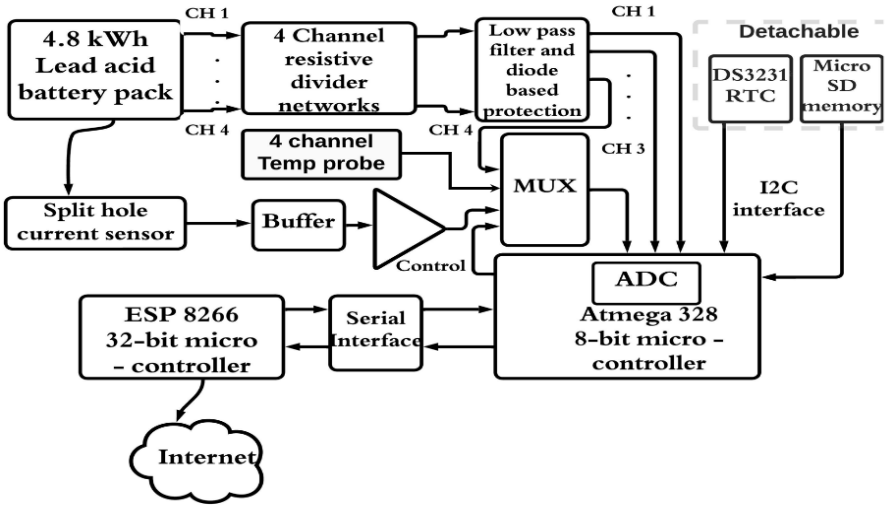

Fig. 1 System-level block diagram of SMDAQ data acquisition system

2.2. SMDAQ Hardware Component and Design

Figure 2 illustrates the schematic diagram of the SMDAQ. The system is built around the ATmega328P microcontroller, selected for its cost-efficiency and balanced features including 16 MHz clock speed, 32 KB flash, 10-bit ADC, and multiple I/O pins (20).A 7805 voltage regulator provides a +5V regulated supply, protected by a 250 mA PTC fuse (1206L025YR), with an LED D1 indicator for power status. Battery voltages are accessed via a five-pin screw terminal connected to a four-series connected battery pack (BTN1–BTN4, GND). Each terminal connects to a voltage divider network with a low-pass filter and Zener diode for protection. Filtered outputs is then applied to the ATMEGA 328 pin 23 (ADC0), pin-24(ADC1), and pin 25(ADC2) for BN1, BN2, and BN3 respectively. Whereas, a filtered signal of BN4 is fed to the pin-14 of CD4051 analog mux.Current is sensed using a WCS1600 non-invasive sensor, buffered by an MCP6002 op-amp and filtered using a 2nd-order Sallen-Key low-pass filter. The filtered current signal connects to pin 13 of the CD4051.Temperature sensing is handled by LM35 probes, each conditioned with an LM358 op-amp in a low-gain configuration.The output of the temperature sensing probes is connected to the pin-15,12,1 and 5 of CD4051 analog mux through the J2 terminal block.The CD4051's select lines (pins 9–11) are controlled by ATmega328P digital pins 2, 3, and 4, with the multiplexer output connected to pin 26 (ADC3).The RTC module (DS3231) provides timestamps via I2C, connected to pins 28 (SCL/ADC5) and 27 (SDA/ADC4) of the ATmega328P. A micro SD card module is used for data backup and DBR implementation, connected via SPI: pins 16–19 ($\overline{SS}$,MOSI, MISO, SCK) to CS, D1, DO, and CLK respectively. For wireless communication, ATmega328P interfaces with Node MCU ESP8266 over UART. Pins 6 (TX) and 11 (RX) of ATmega328P connect to D6 and D5 of ESP8266 for bidirectional battery data transmission over IEEE 802.11.

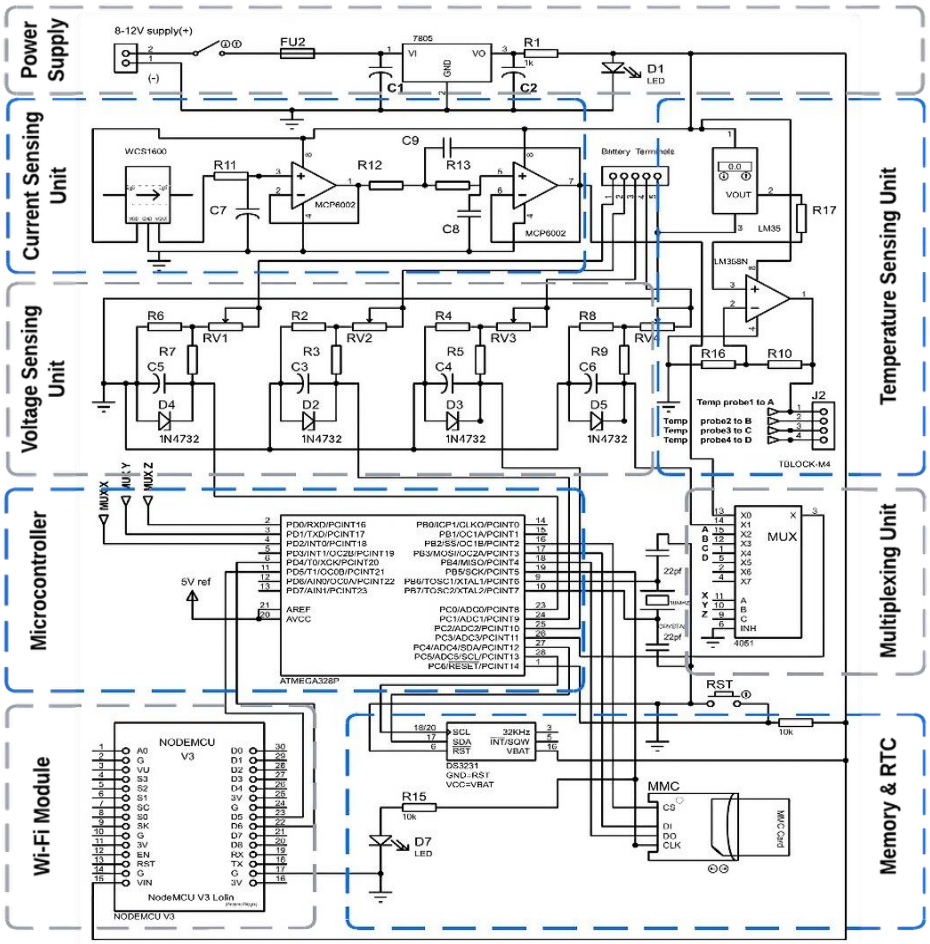

Fig. 2 Schematic diagram of SMDAQ

2.3. Principle Operation of SMDAQ for SOH Monitoring

The SMDAQ is developed to optimize performance and monitor the health of series-connected PbA battery packs. Employing methods like node voltage subtraction, it guarantees accurate measurements across a wide range of battery voltage. While dual-polarity non-invasive current monitoring detects irregularities such as overcharging or excessive discharging, protecting battery longevity. Temperature monitoring analyzes thermal behavior during charging and discharging to monitor abnormality. A calibration process is conducted with respect to theoretical ADC values with practical measurements and also addressing nonlinearities, minimizing errors, and ensuring consistent system performance. Therefore SMDAQ delivers accurate voltage, current, and temperature monitoring for reliable battery management of E3W.

2.3.1. Voltage measurement

In SMDAQ, the node voltage subtraction method is employed to calculate individual voltages in a four-series connected PbA battery pack. The high-potential battery node voltage is measured first, followed by the next lower node. The individual battery voltage is then obtained by subtracting the lower node voltage from the higher. Using Equations 1, 3, 5, and 7, total node voltages are determined to ensure safe operation at 80% DOD. Individual voltages are derived through sequential subtraction using Equations 2, 4, and 6, enabling precise monitoring of each battery's performance.

$$BTN_1 = \sum_{i=1}^{4} B_i \quad \text{where } 45.84\text{ V} \le \sum_{i=1}^{4} B_i \le 66\text{ V} \tag{1}$$

Where 45.84V: Minimum voltage at maximum discharge level of the battery pack.
66V: Maximum voltage at 10% above the absorption stage charging level of the battery pack.

$$B_1 = BTN_1 - \sum_{i=2}^{4} B_i \tag{2}$$

$$BTN_2 = \sum_{i=2}^{4} B_i \tag{3}$$

$$B_2 = BTN_2 - \sum_{i=3}^{4} B_i \tag{4}$$

$$BTN_3 = \sum_{i=3}^{4} B_i \tag{5}$$

$$B_3 = BTN_3 - B_4 \tag{6}$$

$$B_4 = BTN_4 \tag{7}$$

The SMDAQ system is calibrated to monitor PbA battery voltages during the absorption and bulk charging phases (14.3–15V), with an extended detection range up to 10% higher to prevent overcharging. Voltage sensing is configured to measure up to 66V for the full pack, assuming a maximum of 16.5V per battery. Calibration is achieved using four resistive divider networks (14:1, 10.6:1, 7.07:1, and 3.55:1) for voltage scaling at BTN1–BTN4. Each divider is followed by a 50 Hz low-pass filter to suppress high-frequency noise and a 1N4732 Zener diode for signal stabilization, ensuring accurate ADC input to the ATMEGA328P.

Figure 3 illustrates the calibration curve showing the relationship between battery node voltage, ADC input, and ADC count using the calibrated voltage sensing unit. The calibration was conducted over a voltage range of 10V to 66V by comparing theoretical and practical ADC count values. At 10V, the theoretical ADC input is 0.72V, corresponding to an ADC count of 143, while the measured count is 146. At 66V, the theoretical input is 4.68V with a count of 945, compared to a measured count of 965. In the low voltage range (10–20V), practical readings closely match theoretical values with a

1.5% error. A slight deviation of 1.8% is noted in the mid-range (20–50V), and a maximum 2% error appears at higher voltages (50–66V) due to noise interference. This calibration reduces discrepancies and ensures sensor accuracy up to 98%, supporting reliable voltage monitoring.

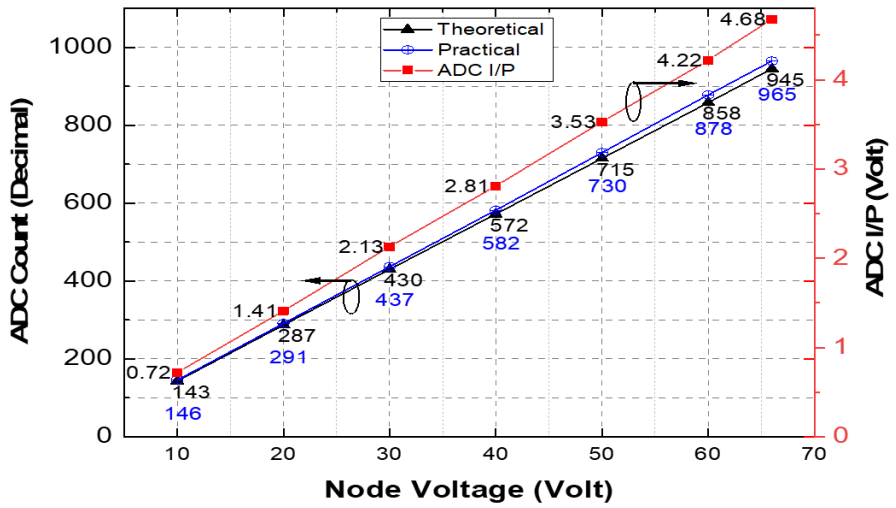

Fig. 3 Graph illustrating the relationship between the node voltage and ADC count along with the ADC input using calibrated voltage sensing unit

2.3.2. Current measurement

In addition to voltage measurement, SMDAQ is equipped to monitor total charging and discharging current of a series-connected PbA battery pack, with an operational range up to 60A and a maximum of 100A. The current sensing module employs a WCS1600 Hall-effect sensor (sensitivity: 22 mV/A at 5V), buffered by an MCP6002 op-amp and filtered using a second-order Sallen-Key low-pass filter. Initially designed with a 4.8 kHz cutoff, the filter is optimized to 112 Hz for effective noise suppression and accurate transient current detection within a 10 ms response time. The filter design ($Q = 0.742$, $\zeta = 0.674$) ensures sharp roll-off, with a phase margin of 145° and a gain crossover frequency of 45.8 Hz, supporting stable and precise current sensing as defined by Equation 8.to produce analog voltage output (V_{out}) of input current (I_{in}).

$$V_{out} = 0.0217 \times I_{in} + V_{offset} \tag{8}$$

The current dependent term 0.0217 is the sensitivity of the current sensor expressed in V/A. V_{offset} represents the sensor base line output voltage when there is no input current ($I_{in} = 0$). Typically, this is half of the input supply voltage (2.5 V for a 5 V supply). To accurately measure the current within the operating range, the decimal equivalent ADC count of the current sensor output voltage is recorded for calibration purposes. The measured current is then obtained using the Equation 9

$$I_{measured} = \left[D_{out} - (2^{N-1} + K_1 \times 2^{N-1}) \Delta V \right]^{S_{UT}^{-1}} - I_{offset} \tag{9}$$

where $I_{measured}$ is current measured by the data logger, D_{out} is digital data output in decimal, K_1 is scaling factor, N is the resolution of ADC of ATMEGA328P, ΔV is the volt equivalent/decimal count, S_{UT} is the sensitivity of the current sensor under test conditions, and I_{offset} is offset current. For this design the value of K_1 and I_{offset} are considered as 0.008 and 1.10 Amp respectively.

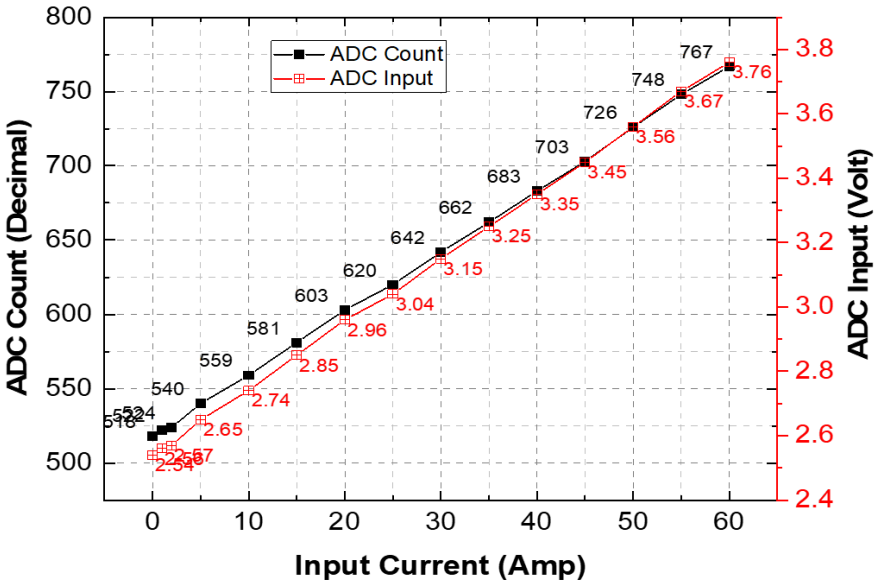

Fig. 4 Graph illustrating the variation of input current with ADC decimal count along with the ADC input using calibrated current sensing unit

Figure 4 illustrates the variation of input current with ADC count using the calibrated current sensing unit. Operating within an ADC range of 512 to 767 for 0–60 A, the sensor shows consistent stepwise increases in ADC count with rising current, confirming accurate analog-to-digital conversion. The stable and proportional voltage increments at each current step validate sensor sensitivity and calibration, enabling detection of transient conditions. The sensing unit maintains low measurement error even at higher currents, effectively capturing current bursts during rapid acceleration or load shifts. This makes the calibrated sensor a reliable tool for monitoring SOH, DOD, and early battery degradation in E3Ws.

2.3.3. Temperature measurement

One key objective of the temperature sensing unit is to monitor thermal behavior and heat generation in PbA batteries, particularly during full charging when exothermic reactions dominate. The construction and implementation of customized temperature sensing probes in SMDAQ are illustrated in Figure 5. A customized four-channel probes are developed to measure electrolyte temperatures between 25°C and 60°C. Each probe

consists of an LM35 sensor connected via CAT-5 cable, insulated with heat-shrink tubing and epoxy, and enclosed in a 316-grade stainless steel tube with thermal silicone paste for accurate heat transfer. Signals are conditioned using an LM358-based non-inverting amplifier (Av = 5.5) and routed through a CD4051B analog multiplexer to a single ADC input for sequential sampling.

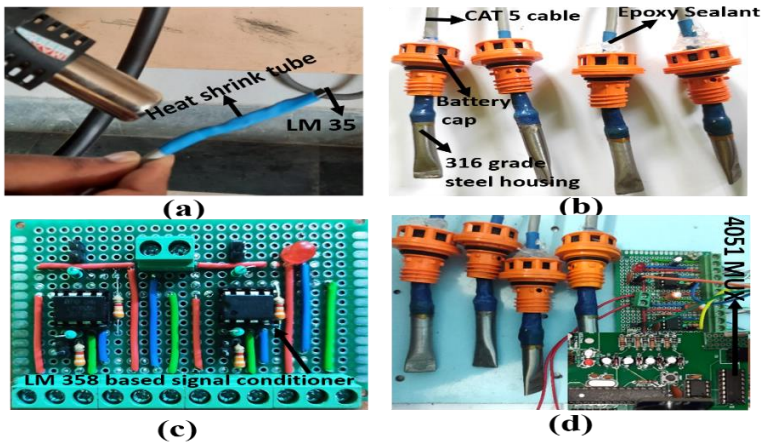

Fig. 5 Photograph depicting the components of the developed prototype (a) temperature sensing probe using LM35 with blue tube encapsulation (b) temperature probe integrated with battery cap, Cat 5 cable and housed in 316 grade steel for protection (c) temperature signal conditioning unit utilizing LM358 (d) comprehensive view of the temperature probe, battery cap, signal conditioning unit, and SMDAQ DAQ system.

This setup minimizes voltage drop and noise while enabling organized logging of individual battery temperatures during charging and discharging, as defined by Equation 10.

$$T_{measured} = \frac{D_{out} \times A_{ref} \times 10^2}{2^n \times K_1} \tag{10}$$

Where T_{measured} is temperature of battery in ºC, D_{out} is ADC count in decimal, A_{ref} is the reference voltage of ADC, n is resolution of ADC and K_1 is scaling factor depends upon gain of the amplifier.

Figure 6 shows the relationship between temperature, ADC decimal count, and ADC input voltage using the calibrated temperature sensing unit. Calibration was conducted over a temperature range of 25°C to 60°C, corresponding to an output voltage span of 1.41 V to 3.3 V from the signal conditioning circuit. The LM35 sensor generates 10.2 mV/°C, which after amplification provides 56 mV/°C. Based on Equation 11 and using a 5 V analog reference for the ADC, the measured counts align well with theoretical predictions showing 282–288 counts at 25°C and 676 counts at 60°C. This confirms the sensor's linear response across the full range. The use of a signal conditioning circuit improves sensitivity and maintains a stable linear relationship between temperature and ADC output.

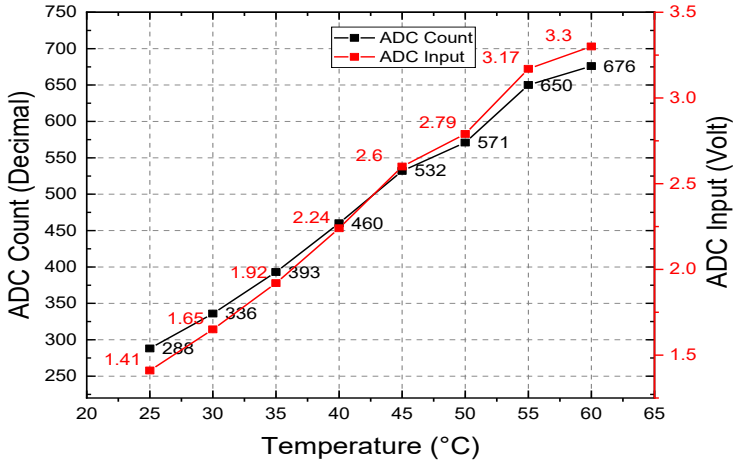

Fig. 6 Graph showing the trend of temperature variation with ADC decimal count along with the ADC input voltage using a calibrated temperature sensing unit.

$$\Delta\text{ADC count} = \frac{56\text{mv/℃}}{4.88\text{mv/count}} \approx 11.5 \text{ counts/℃} \tag{11}$$

The systematic approach of calibration techniques applied to the SMDAQ DAQ ensures a linear, accurate and robust real-time measurement of the battery parameters of the E3W vehicle. As discussed, the calibration of the voltage sensor unit achieves 98% accuracy for the voltage measurement while the current sensing unit provides precise high-current measurements with 98.6% accuracy and the temperature sensing unit offers 98% accuracy across the desired range.

2.4. Voltage-Current Based SOH Estimation Using RMSE and Kalman Residuals

The State of Health (SOH) of onboard PbA batteries in E3Ws is evaluated by examining both static and dynamic behaviors during operation. Figure 7 presents the SOH estimation flowchart, highlighting key processes including data acquisition, current sensing, DOD computation, RMSE and Kalman residual estimation, and discrepancy evaluation. RMSE captures static discrepancies by measuring the average deviation between observed and reference voltages across different DOD levels. In contrast, Kalman residuals represent dynamic discrepancies by quantifying the difference between measured voltage and the voltage estimated by a Kalman filter during real-time drive cycles. Combining these two metrics allows for a comprehensive SOH assessment, covering both steady-state and transient load conditions typical of E3W usage. A weighted evaluation approach highlights cases where both static and dynamic degradation indicators align, ensuring a more robust and accurate estimation of battery health.

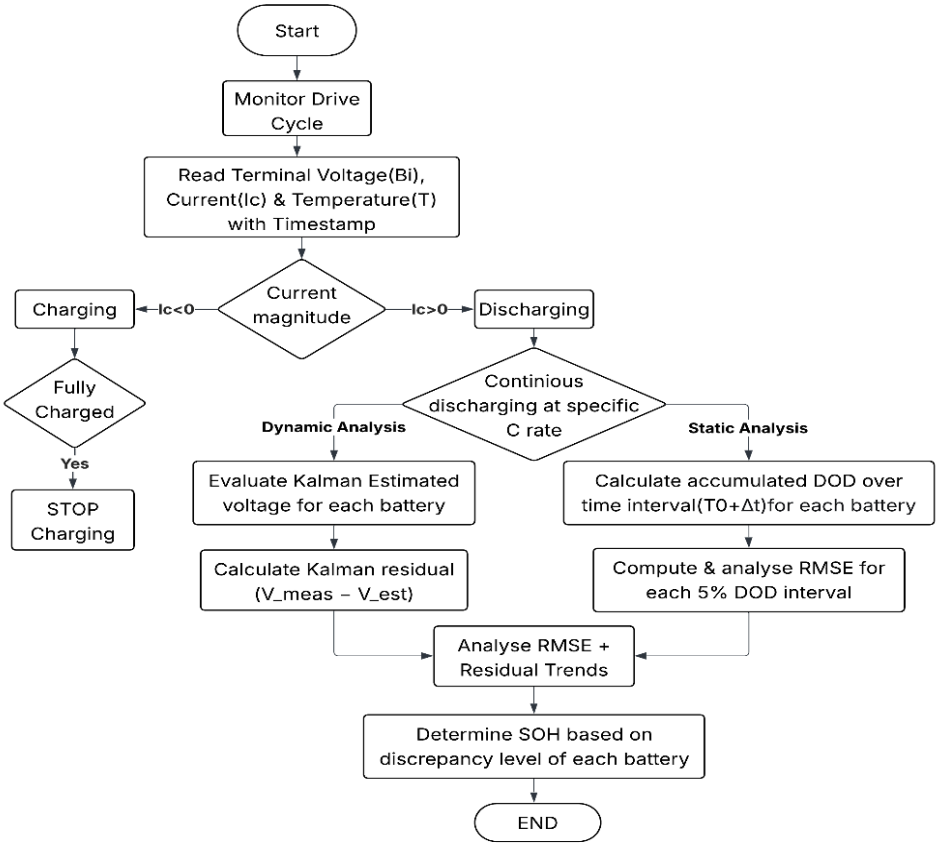

Fig. 7 SOH estimation flowchart using RMSE and Kalman residual analysis

2.4.1. Drive cycle-based DOD computation for SOH evaluation

Battery performance under real-world driving is evaluated through discharge current, the key performance parameter shaped by drive cycle demands. Feature parameters like DOD in ampere-hours (Ah), representing cumulative energy use, are extracted from these discharge profiles for accurate SOH estimation. Real-time monitoring with SMDAQ enables precise DOD tracking and early fault detection across the E3W drive cycle, with net discharge current measured at discrete intervals using Equation 12.

$$\int_{t_1}^{t_n} I_D(t)dt = \frac{\Delta t}{2}[I_D(t_1)+2I_D(t_2)+3I_D(t_3)+\ldots I_D(t_n) \quad (12)$$

$I_D(t)$ = instantaneous discharge current over the time interval, $t_0 + \Delta t$, t_n = total driving lap sample time.The integration of current over time provides a continuous understanding of battery utilization during different phases of the drive cycle, such as acceleration, deceleration, and idle periods. t_1 and t_n are the time taken for driving lap D_{L1} and D_{Ln} respectively. The driving lap time is measured using Equation 13 and 14.

$$T(n_i) = \sum_{i=1}^{n} T_i + \sum_{i=n+1}^{N} T_i \quad \text{for } N-(n) \le 8 \tag{13}$$

$$T(n_i) = \sum_{i=1}^{n} T_i \quad \text{where} \quad \sum_{i=n+1}^{N} T_i \to 0 \quad \text{for } N-(n) > 8 \tag{14}$$

Where n= number of non zero magnitude of current and N= total number of lap sample count. The ampere-hour discharge is then calculated using the coulomb counting method, as represented by Equation 15.

$$S_{OC}(t) = 100\% - D_{OD}(t) \tag{15}$$

Where $S_{OC}(t)$ = state of charge, D_{OD} (t) =depth of discharge at time t. The discharging current I_D is measured using the current sensing unit of SMDAQ in discrete time intervals. The quantitative measure of the change in Depth of Discharge (ΔD_{OD}) over a specific time (Δt) for a given discharge current profile is calculated using Equation 16

$$\Delta D_{\mathrm{OD}} = \frac{\int_{t_0}^{t_0+\Delta t} I_{\mathrm{D}}(t)\,dt}{Q_{\mathrm{rated}}} \times 100\% \tag{16}$$

Where Q_{rated} = rated capacity of the battery and I_D (t) = instantaneous discharge current over the time interval $t_0 + \Delta t$.

By evaluating ΔD_{OD} over time, the equation facilitates real-time tracking of how much energy is consumed during operation, making it essential for dynamic conditions such as rapid acceleration or varying load in E3W vehicles. As time elapsed and the E3W covers a higher distance therefore accumulated DOD is represented by Equation 17.

$$D_{OD}(t) = D_{OD}(t_0) + \Delta D_{OD} \tag{17}$$

The equation provides the evaluation of individual batteries in a pack by comparing their $D_{OD}(t)$, assisting in identifying discrepancies that could indicate performance degradation or faults.

2.4.2. Dynamic voltage tracking using Kalman residual analysis

PbA battery performance in E3Ws is highly influenced by dynamic factors such as acceleration, load shifts, and varying drive cycles, leading to fluctuations in load terminal voltage. Traditional degradation models fall short under such conditions due to static assumptions and dependence on historical data. A data-driven Kalman Filter (KF) approach overcomes these limitations by incorporating real-time sensor data, filtering noise, and adaptively estimating SOH by comparing real-time voltage and current data from SMDAQ with the predicted values. The Kalman-estimated voltage (x_k) enables accurate tracking of battery health and early fault detection under fluctuating discharge conditions, as represented in Equation 18.

$$x_k = \mathrm{A}x_{k-1} + \mathrm{B}u_k + w_k \tag{18}$$

Where A= state transition matrix, defining how battery voltage changes due to past values, external factors like current and temperature, B= control matrix, representing the influence

of external inputs on voltage, u_k = external input vector incorporating current (I) and temperature (T) variation at k_{th} time instance and represented by $[I_k, T_k]^T$, w_k = process noise, accounting for system uncertainties.

Before incorporating new sensor data, the predicted voltage is given by Equation 19

$$\widehat{\hat{x}_k} = A\hat{x}_{k-1} + B_1 I_k + B_2 T_k + w_k \tag{19}$$

Based on sensor data, electrolyte temperature in PbA batteries varies only 3–5% during discharge, even under E3W drive cycles. Since its impact on prediction accuracy is minimal, it is excluded from the model to reduce complexity and focus on dominant factors (I_k) enhancing accuracy and performance.

Once new measurements are available, the estimated voltage is updated by Equation 20

$$\hat{x}_k = \widehat{\hat{x}_k} + k_g(R_m - H\widehat{\hat{x}_k}) \tag{20}$$

Where k_g = Kalman gain, determining how much correction is applied, R_m = measured voltage from SMDAQ which includes voltage fluctuation and noise due to drive cycle, H= observation matrix, mapping the predicted state to the measured output.
The kalman residual (e_k) is represented by Equation 21

$$e_k = (R_m - H\widehat{\hat{x}_k}) \tag{21}$$

The Kalman filter residual quantifies the discrepancy between the measured and predicted voltages. By analyzing these residuals across four PbA batteries, early degradation trends are detected.

2.4.3. Static RMSE analysis over DOD intervals

In addition to dynamic SOH analysis, a static evaluation is performed using Root Mean Square Error (RMSE) computed at every 5% Depth of Discharge (DOD) interval up to 80%. At each interval *DOD*, *k* and *RMSE* quantifies the deviation between the measured terminal voltage $V_{meas,i}^{DOD,k}$ and the standard reference voltage $V_{ref,i}^{DOD,k}$ and expressed by Equation 22

$$RMSE_{DOD_k} = \sqrt{\frac{1}{n}\sum_{i=1}^{n}\left(V_{meas,i}^{DOD,k} - V_{ref,i}^{DOD,k}\right)^2} \tag{22}$$

Where, $V_{meas,i}^{DOD,k}$ = measured terminal voltage at the i^{th} sample within the k^{th} DOD interval. $V_{ref,i}^{DOD,k}$ = Reference (standard) terminal voltage at the same DOD. n = Number of voltage samples in that DOD interval.

This analytical approach identifies voltage deviations at specific DOD levels (e.g., 40%, 60%, 80%), enabling early detection of stress or degradation zones. The dual-method SOH framework combining Kalman filtering for dynamic deviations and RMSE for static errors at 5% DOD intervals enhances accuracy and robustness in monitoring E3W battery health under real-world conditions.

3. SOFTWARE ARCHITECTURE AND SYSTEM OPERATION

In SMDAQ, the ATMEGA328P is programmed in embedded C. Additionally, to perform step-by-step debugging, examine variables, and identify issues during development executable linkable file (elf) and assembly code are extracted to optimize the program for memory and performance. The coding part is divided into three sections. The first section describes the program sizing for the measurement of battery parameters using ATMEGA328P. The second part focuses on integrating cloud server with data transmission and backup mechanism and the last section illustrates the development of an application programming interface (API) for real time monitoring of battery parameter.

3.1. Program Sizing and Timing Computation

The program sizing and T-state analysis of SMDAQ DAQ are presented in Table 2. This analysis is performed to optimize code and improve memory performance. The program requires 23,068 bytes of program memory and 1,528 bytes of data memory, with 33 arithmetic and logical instructions, 148 branch instructions, and 542 data transfer instructions contributing to a total of 1,294 T-states. These result in an execution time of 80.8µs. The distribution of T-states shows that data transfer instructions dominate (701 T-states) due to the frequent transfer of data between sensors, memory, and communication modules followed by branch (551 T-states) and arithmetic/logical instructions (42 T-states). This highlights optimizing real-time data handling and branching logic to enhance performance and reduce resource usage of SMDAQ.

Table 2 Program sizing and T-state analysis of SMDAQ DAQ

Program Parameter	Unit
Program memory requirement	23068 byte
Data memory requirement	1528 byte
Total no of arithmetic and logical instruction	33
Total no of branch instruction	148
Total no of data transfer instruction	542
Total T-state	1294
Total execution time	80.8µs
T-state(arithmetic and logical instruction)	42
T-state(Branch instruction)	551
T-state(data transfer instruction)	701

3.2. Data Backup and Retransmission (DBR) with Cloud Integration

Figure 8 illustrates the SMDAQ data backup and transmission mechanism. Sensors operate at a 10 Hz sampling rate, capturing voltage, current, temperature, and time. Every 20 samples are aggregated and formatted as a JSON string to reduce transmission overhead, then sent via HTTP POST to a PHP Web Server and stored in an Amazon RDS Cloud Database through a RESTful API. An E3W vehicle authorization token ensures secure access, while a query manager enables real-time and historical data retrieval. In real-time mode (Thread 1), data is sent directly to AWS IoT core. If the network fails, data is locally stored on a memory card with timestamps. Once connectivity is restored, Thread 2 transmits the stored data, ensuring no loss. This dual-threaded approach optimizes real-

time monitoring, guarantees data integrity, and enhances fault tolerance in E3W battery health assessment.

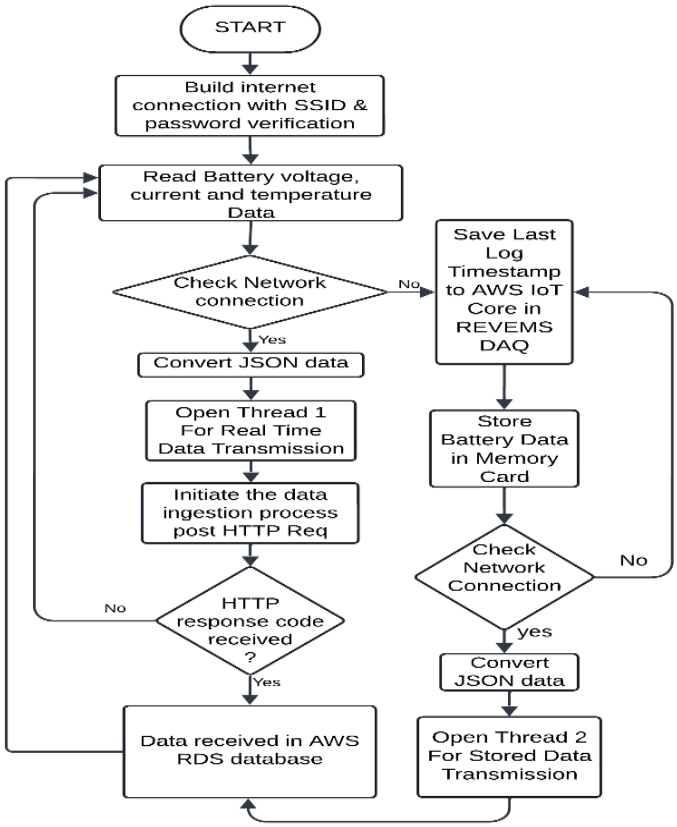

Fig. 8 Data backup and transmission mechanism of SMDAQ

3.3. Application Programming Interface Design and Data Visualization

A customized battery parameter monitoring user interface (UI) is developed using the Kotlin programming language, utilizing its interoperability with Java for seamless integration. It employs HTTP URL connections to interact with an AWS RDS server, allowing real-time API-based data retrieval. The UI manages user inputs, processes battery-related data, and dynamically displays server responses. The backend is built using PHP and MySQL, ensuring secure user authentication and efficient session management for the E3W vehicle. Figure 9 illustrates the SMDAQ API decision-making process using color-coded voltage indicators for battery health assessment. Red indicates deep discharge (DOD > 85%) when voltage drops below 11.40V. Yellow marks moderate discharge (around 50% DOD) with voltages between 11.40V and 11.95V. Green represents a healthy charge state (50%–100% SOC) with voltages above 11.95V, aligning with standard PbA battery guidelines. By displaying real-time voltage levels alongside current and

temperature data, SMDAQ enables timely intervention, enhances operational reliability, and extends battery life for effective monitoring of E3W onboard PbA batteries.

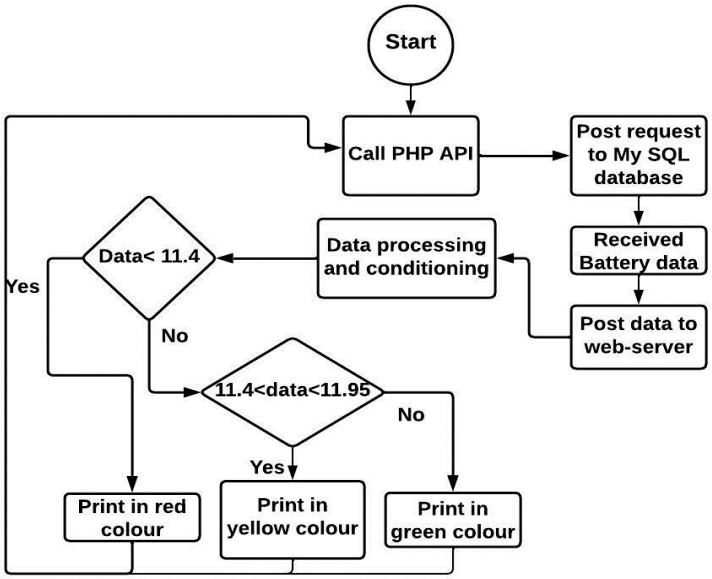

Fig. 9 Flowchart illustrating the decision making process for voltage level classification with colour coded outputs

4. Results and Discussion

An experimental setup is arranged using the developed SMDAQ DAQ module connected to four series-connected tubular PbA batteries (each 12V, 100Ah, C20 rating). These 4.8kWh series connected batteries provide the electrical energy required to drive the 900-watt, 3000 RPM, 48-volt BLDC electric motor and deliver power to sustain acceleration, and cruising of E3Ws. Figure. 10. Illustrates the prototype of SMDAQ DAQ integrated into an E3W for monitoring battery parameter. To measure the battery health and the post-impact on batteries under varying charging and discharging conditions, different drive cycle of L3 type E3W over extended driving periods is considered. Drive cycles for such vehicles are considered in typical rural and semi-urban driving scenarios and characterized by speed variability idle to peak speeds (typically 25–30 km/h), acceleration and deceleration, idle time, constant speed sections, and battery load (energy consumption during various phases of the drive cycle).

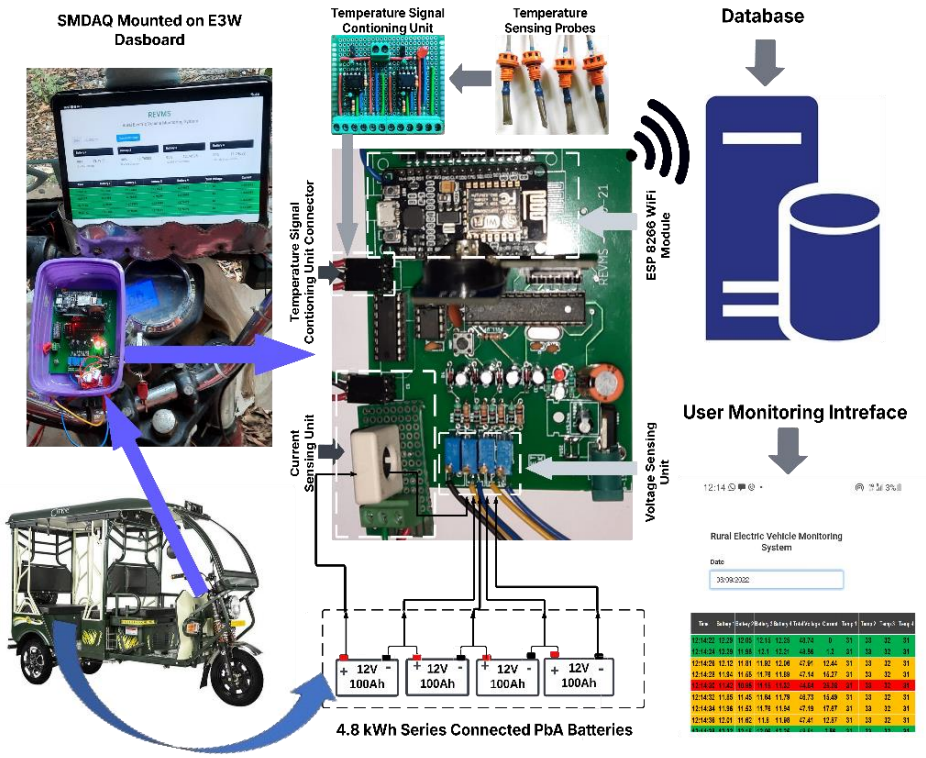

Fig. 10 Prototype of SMDAQ data logger integrated into Electric Three Wheeler (E3W)

4.1. Verification of Voltage and Current Accuracy Using SMDAQ

Real-time experiments validate SMDAQ voltage data by comparing it with standard test meter readings from full charge to 80% DOD during E3W operation. Voltage and discharge current of each battery in the 1P4S pack are measured at 60-second intervals and matched against SMDAQ interface data to ensure accuracy. Figures 11 and Figure 12 validate SMDAQ's accuracy by comparing its voltage and current readings with a test meter over different drive cycle intervals. In Figure 11, SMDAQ effectively tracks voltage fluctuations between 12.69V and 11.66V across the 0–2220 sec drive cycle interval, capturing drops at 540 sec, 1500 sec and 2220 sec and peaks at 1740 sec. Figure 12 presents current readings over 0–1980 sec, where SMDAQ records sharp spikes above 50A at 720 sec and 1800 sec, as well as low-current conditions, closely matching the test meter. The alignment confirms SMDAQ's reliability in real-time PbA battery current monitoring.

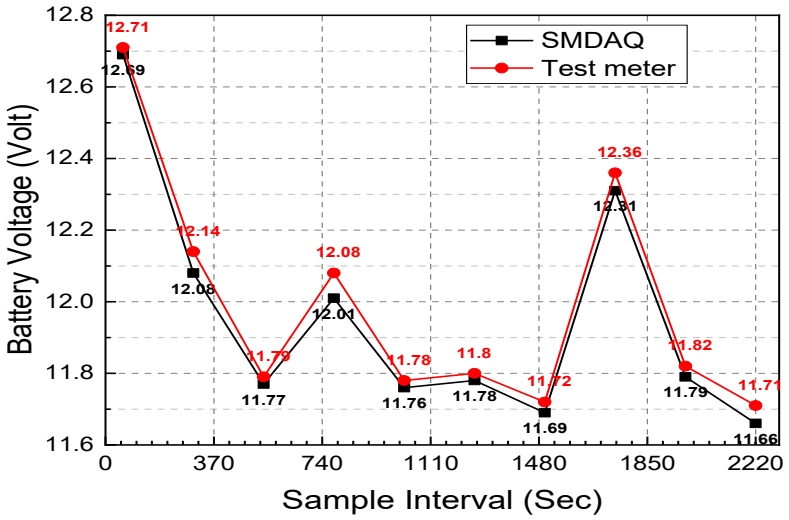

Fig. 11 Voltage vs. time reading of batteries as recorded by SMDAQ and the test meter

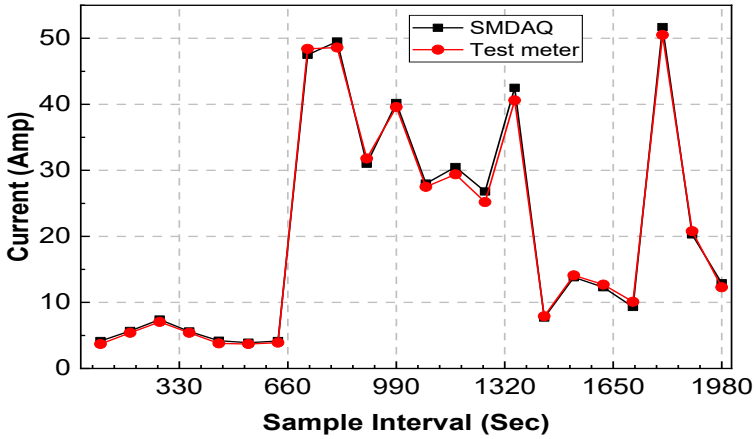

Fig. 12 Current vs. time reading of batteries as recorded by SMDAQ and the test meter

4.2. SOH Assessment Using Kalman Filter Residual Analysis

An experiment is conducted to evaluate battery performance under various drive cycles during an extended discharging period at 80% Depth of Discharge (DOD). The test covered driving laps from 1 km to 75 km, considering real-world conditions where battery performance is influenced by driver habits, vehicle load variations, and voltage drops due to increased current demand. Figure 13 presents the SOH estimation using Kalman filter residual voltage analysis over time for four PbA batteries. Residuals for Battery 1 and Battery 3 are the highest, reaching 0.56 V and 0.61 V by 15:32, indicating severe degradation. The residuals for Battery 4 are lower than Battery 1 and Battery 3 but still

increase gradually. By 15:32, its residual reaches 0.35V, meaning it is moderately degrading. Battery 2 remains the most stable at 0.30V. Increasing residual trends confirm voltage drops, demonstrating the Kalman filter's effectiveness in tracking SOH degradation in real-time, making it a reliable method for E3W battery health monitoring.

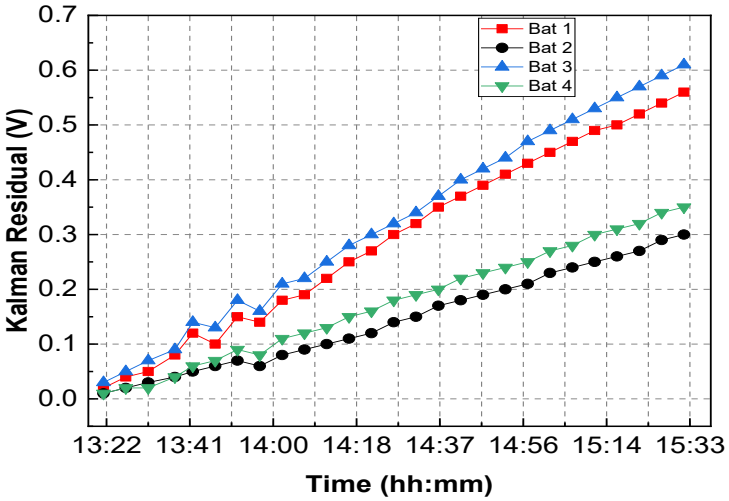

Fig. 13 Evaluation of SOH using discharge cycle characteristics (kalman filter residual voltage vs time) for four batteries in a E3W drive cycle

4.3. Voltage Response Analysis under Varying Discharge Rates

Figure 14 illustrates the influence of vehicle dynamics on battery performance and discharging behavior of batteries under varying discharging rates. The voltage profile of a 1P4S battery configuration (comprising four 12V, 100Ah batteries: B1, B2, B3, and B4) is continuously monitored over an extended drive cycle to analyze voltage variations, imbalances, and transient behaviors under varying load conditions. The critical voltage threshold of 11.46V, at 80% DOD level marked on the graphs, highlights the risk of over-discharge. Figure 14.a illustrates the impact of rapid acceleration in congested traffic on E3W operation. Frequent stops and acceleration caused transient current spikes at a 0.5C discharge rate, straining Battery 1 and Battery 3, leading to faster energy depletion and significant voltage sag below 10.5V for both. Figure 14.b and Figure 14.c illustrate smooth traffic conditions with minimal speed variations and stops, where batteries discharge at lower C-rates (0.15C–0.2C). Battery 2 and Battery 4 remained balanced with Battery 2 maintaining a higher voltage and slower energy depletion. Conversely Battery 1 and Battery 3 exhibited a sharp voltage drop below the critical threshold. In moderate traffic, E3W dynamics involve more frequent starts and stops with higher acceleration bursts than in smooth traffic, increasing current demand. This occasionally creates transient short circuits, drawing over 0.3C at various points in the drive cycle, depicted in Figure 14.d. Battery 1 and Battery 3 are most affected, with terminal voltages dropping below 10.8V and 11.0V respectively, increasing the risk of damage due to higher internal resistance. Conversely, Battery 2 and Battery 4 maintain voltages around 11.2V under similar DOD

conditions. At higher C-rates, the performance gap between the strongest and weakest batteries is widened and more noticeable. The consistently poor performance of Battery 1 and Battery 3 suggests it should be inspected or replaced to improve overall pack performance.

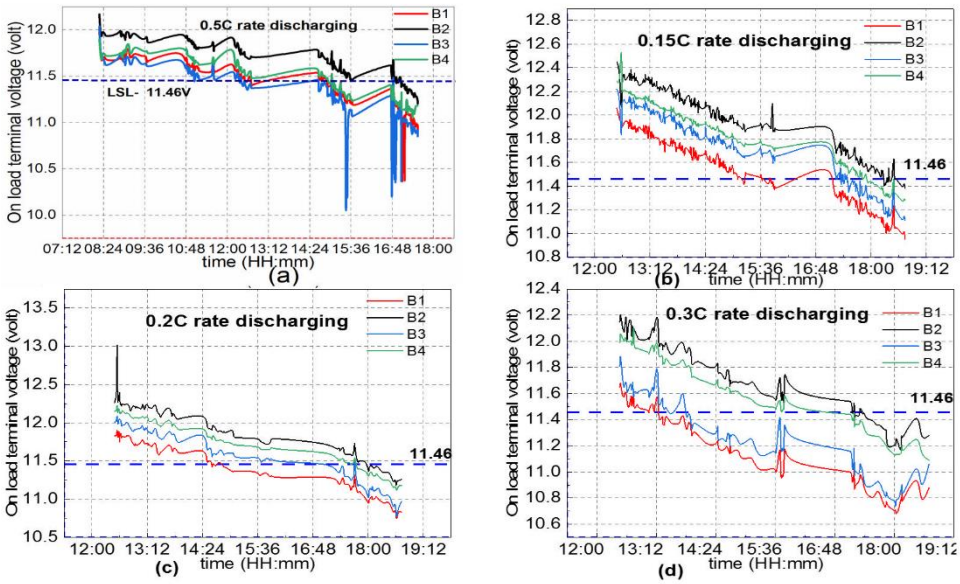

Fig. 14 Voltage and discharge characteristics of batteries under different traffic conditions: (a) transient current at 0.5C discharge rate (b) 0.15C-rate discharge (c) 0.2C- rate discharge and (d) 0.3C-rate discharge.

4.4 RMSE-Based Deviation Analysis at Varying DOD

Table 3 illustrates the RMSE values change across different DOD levels for the four tested batteries. At low DOD levels (5%–20%), all batteries perform well with very low RMSE, showing stable voltage behavior. Between 25% and 55%, Battery 1 and Battery 3 start to Show a gradual increase in RMSE, reaching up to 0.45 V. This suggests early signs of performance decline, while Battery 2 and Battery 4 remain stable with low errors. A sharp increase is seen from 50% to 60% DOD, where Battery 1 jumps from 0.31 V to 0.73 V, and Battery 3 from 0.42 V to 0.56 V. This sudden rise marks the beginning of clear voltage prediction errors. At higher DOD levels (65%–80%), the RMSE for Battery 1 reaches a peak of 1.21 V, and Battery 3 rises to 0.84 V. In contrast, Battery 2 and Battery 4 continue to show smaller changes, staying below 0.41 V. These results suggest that Battery 1 and Battery 3 degrade faster and are more affected by deep discharges. The higher RMSE values are likely caused by increased internal resistance, voltage sag, and aging effects, which impact voltage accuracy under load.

Table 3 RMSE analysis of tested batteries at different DOD level

DOD (%)	Battery 1	Battery 2	Battery 3	Battery 4	Observation
5	0.03	0.07	0.18	0.03	All batteries stable; low deviation
10	0.02	0.02	0.20	0.04	
15	0.03	0.08	0.42	0.28	
20	0.13	0.12	0.28	0.11	
25	0.16	0.14	0.32	0.08	Battery 1 & 3 show early rise; B2 & B4 stable.
30	0.15	0.12	0.24	0.09	
35	0.13	0.09	0.27	0.14	
40	0.11	0.12	0.26	0.12	
45	0.17	0.18	0.3	0.12	
50	0.31	0.06	0.42	0.11	
55	0.41	0.04	0.45	0.07	
60	0.73	0.20	0.59	0.26	B1 & B3 degrade sharply; B2 & B4 hold steady.
65	1.21	0.41	0.84	0.41	
70	1.13	0.38	0.64	0.40	
75	1.05	0.37	0.69	0.39	
80	0.97	0.32	0.62	0.38	

4.5 Integrated RMSE-Kalman Residual Analysis for Battery SOH Estimation

Table 4 illustrates the combined RMSE–Kalman residual analysis and final SOH interpretation of batteries, applying threshold limits of RMSE (upper: 0.50, lower: 0.35) and Kalman residual (upper: 0.25, lower: 0.15). Battery 1 exceeds both thresholds significantly, with RMSE at 0.83 and residual at 0.293, indicating advanced degradation due to poor voltage consistency and dynamic instability. Battery 3 also shows degradation, with moderate RMSE (0.60) and high residual (0.284), suggesting declining performance under both static and dynamic conditions. Battery 4, while within the RMSE limit (0.29), shows a moderate residual (0.199), pointing to slight aging likely driven by early dynamic response delay. In contrast, Battery 2 remains well within both thresholds, RMSE at 0.26 and residual at 0.145 confirming a healthy SOH. This dual-metric evaluation enhances diagnostic accuracy by capturing both steady-state deviation and transient behavior.

Table 4 Combined RMSE–Kalman residual analysis and SOH interpretation of batteries

Battery	Avg. RMSE (50–80% DOD)	Kalman Residual	Combined Interpretation	Condition	Battery SOH
Bat1	0.83	0.293	High RMSE + High Residual	RMSE > 0.50 and Residual > 0.25	Degraded
Bat 2	0.26	0.145	Low RMSE + Low Residual	RMSE < 0.35 and Residual < 0.15	Healthy
Bat 3	0.60	0.284	Moderate RMSE + High Residual	RMSE > 0.50 and Residual > 0.25	Degraded
Bat 4	0.29	0.199	Low RMSE + Moderate Residual	RMSE < 0.35 and Residual > 0.15	Slightly Aged

4.6 Temperature Monitoring

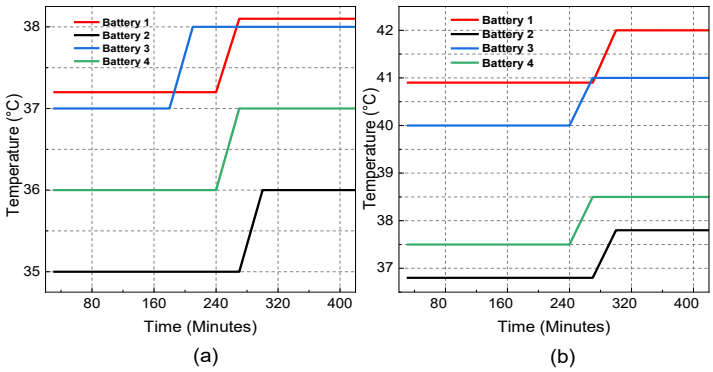

Fig. 15 Plot showing temperature characteristics (temp vs time) of batteries: (a) during discharging condition; (b) during charging condition

Figure 15.a presents temperature profiles during a 400-minute discharge, showing that Battery 2 and Battery 4 operated at lower temperatures than Battery 1 and Battery 3. As shown in Figure 15.b, during charging, the electrolyte temperatures of Battery 1 and Battery 3 increased by 8–10% due to exceeding the absorption voltage threshold (14.8V), while Battery 2 and Battery 4 showed only a 4% rise, remaining within optimal charging limits.

4.7 SMDAQ Battery Health Monitoring Interface

Figure 16 (a) represents SMDAQ system display mounted on the E3W dashboard showing real-time battery monitoring data. The screenshot of the SMDAQ mobile user interface (UI) is shown in Figure 16(b). The snapshot shows colour-coded information for quick status assessment where Battery 1 and Battery 3 voltage drops below 11.4Vand the pack voltage falls below 45.84 V,the interface turns red, indicating a critical condition. A

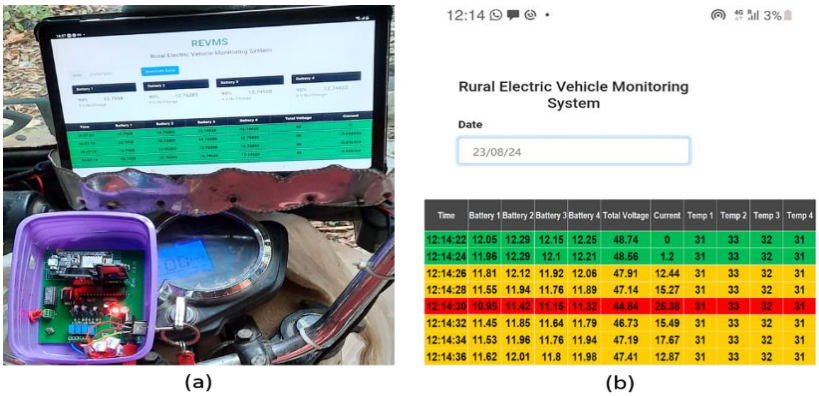

Fig. 16 (a) SMDAQ system display mounted on the E3W dashboard (b) mobile user interface of the SMDAQ battery health monitoring system displaying real-time battery parameters.

yellow warning is displayed when the battery voltage ranges between 11.4V and 11.95V, signaling moderate discharge. When all batteries exceed 11.95V, the interface turns green, indicating that the batteries are within a safe operational range. This color-coded approach provides an efficient method for users to monitor and maintain battery health effectively. Additionally, SMDAQ functions as a data-driven performance forecasting tool for battery health monitoring and provides decisive findings for E3W owners and battery manufacturers to diagnose battery issues early and prevent unexpected failures of PbA batteries.

4.8 Comparison of SMDAQ Hardware with Existing Prototypes for Battery Health Estimation

Table 5 illustrates the comparative analysis with other state-of-the-art works and prediction methods, highlighting key advancements in this research.

Table 5 Comparative analysis with other state-of-the-art works and prediction methods

Parameters	Ref [31]	Ref[32]	Ref[33]	Ref[34]	Ref[35]	This work
Hardware design	devboard-based	Multi-dev board-based	MCU+MUX+ sensors+balancing circuit	Multi-dev board-based	Multi-dev board-based	Custom PCB + integrated MCU+MUX +filters+sensors + signal cond.
Battery under test	Li-Ion,48V, 28Ah	PbA SMF, 12V,26Ah	18,650Li-ion, 3.7V,1.4Ah	PbA ,12V Above 65Ah	18,500Li-ion,3.7V, 2Ah	1P4S PbA,48V, 4×100Ah 4.8kWh
MCU	Two ESP 8266 board	ATmega328, ARM 7, ESP 8266	ATmega 328, ESP 8266	ATmega128a WizFi210	ARM Cortex-M4F	ATmega328 ESP 8266
Voltage Sensor	Simple voltage divider	Generic divider module	Simple voltage divider	BQ34Z110 IC	Generic divider module	4 channel voltage divider
Current Sensor,	LANTIANRC	ACS712	Opto-coupler and IRLZ44N	BQ34Z110 IC	ACS712	WCS 1600 22mv/A
Temp Sensor	DHT 11	DHT 22	10kΩ Thermistor	Chip cap-D sensor	DHT 11	Multiplexed LM 35 probes
Load	BLDC,550 W,48V	Rheostat,50Ω, 5A	2Ω,discharged through IRLZ44N	Not given	Bulb	E3W BLDC, 900W,48V
Max Volt, current, Temp	46V,16A, 27°C	25V,30A, 80°C	34V,33A, 33°C	65V, not given	3.7V,1A,	66V(±2%) 60A(±1.5%) 42°C(±2°C)
Custom data visulization	Limited	Limited	Moderate	Full	Limited	.mazonRDS&RESTfulAPI
Hosting	Thing Speak cloud servers	Raspberry Pi as a local server	HTML and CSS, a web server	UDP Server Socket-Based	Cool Term based local server	A PHP Web Server with Amazon RDS
SOH prediction methods	No	Estimated SOC + MSE	LSTM + RNN architecture	State of charge	LSTM + RUL prediction	DOD analysis+ Kalman residual +RMSE
SOH assessment capability	No	Static	Static	Static	Limited dynamic profiling	Static and dynamic
Drive cycle & transient analysis	Not supported	Not supported	No real time profiling	Partially supported	Partially supported	Fully supported

Unlike previous lab-based studies, this work uses an E3W BLDC motor under real-world drive cycles, capturing actual discharge profile instead of relying on controlled conditions. A custom PCB integrates the MCU, MUX, filters, sensors, and signal conditioning, improving accuracy over conventional designs. The system supports 66V (±2%), 60A (±1.4%), and 42°C (±2°C), making it suitable for high-power applications. Real-time data access and cloud backup are enabled via a RESTful API and Amazon RDS, with support for both online and offline modes for improved reliability. A combined Kalman Residual and RMSE approach with DOD tracking allows early detection of degradation, enabling predictive maintenance and accurate SOH estimation. This practical, scalable solution enhances battery monitoring for E3W applications.

5. CONCLUSION

A customized, affordable SMDAQ system has been designed and implemented. Using direct measurement techniques SMDAQ diagnoses the state of health of PbA batteries, which serve as the primary power source for E3W vehicles. Through a structured design methodology, the SMDAQ monitors, calibrates, and evaluates key design attributes including battery voltage, current, and temperature of four series-connected lead-acid (PbA) batteries under charging and discharging conditions in real-time. The prototype delivers an impressive accuracy of 98.6%. Extensive field testing across various E3W drive cycles validates that SMDAQ provides comprehensive battery performance analysis, specifically monitoring C-rate discharge behavior across diverse traffic conditions. It captures voltage variations, transient current spikes, and imbalances between batteries, enabling early detection of performance discrepancies. The dual approach, Kalman filter residual with RMSE analysis enhances predictive monitoring by identifying potential battery health issues. Custom temperature sensing probes track thermal variations during overcharging, preventing overheating risks. The user-friendly interface provides real-time battery health updates, allowing proactive maintenance to extend battery life. SMDAQ minimizes the impact of a single defective battery on the entire pack by enabling timely detection and replacement. Additionally, its ability to assess the influence of vehicle dynamics and traffic patterns on battery performance makes it a valuable tool for predictive maintenance. This robust system supports both E3W owners and battery manufacturers in diagnosing issues, optimizing performance, and improving overall reliability and efficiency.

REFERENCES

[1] G. Wu, A. Inderbitzin, and C. Bening, "Total Cost of Ownership of Electric Vehicles Compared to Conventional Vehicles: A Probabilistic Analysis and Projection Across Market Segments", *Energy Policy*, vol. 80, pp. 196-214, 2015.

[2] A. Pandey and C. Venkataraman, "Estimating Emissions From the Indian Transport Sector With On-Road Fleet Composition and Traffic Volume", *Atmos. Environ.*, vol. 98, pp. 123-133, 2014.

[3] R. Hema and M. J. Venkatarangan, "Adoption of EV: Landscape of EV and opportunities for India," *Measurement: Sensors*, vol. 24, p. 100596, 2022.

[4] S. N. Saxena, "Revolution in Growth of Three-Wheeler Electric Vehicles in India Providing Job Opportunities to Semi-Skilled and Unskilled People" *J. Global Tourism Res.*, vol. 4, no. 2, pp. 117-126, 2019.

[5] P. T. Moseley and D. A. J. Rand. "The Valve-Regulated Battery—A Paradigm Shift in Lead-Acid Technology." In *Valve-regulated lead-acid batteries*, pp. 1-14, Elsevier, 2004.

[6] G. Adu-Gyamfi, H. Song, B. Obuobi, E. Nketiah, H. Wang and D. Cudjoe, "Who Will Adopt? Investigating the Adoption Intention for Battery Swap Technology for Electric Vehicles", *Renew. Sustain. Energy Rev.*, vol. 156, p. 111979, 2022.
[7] C. R. Lashway and P. Idowu, "A Test System for Advanced Lead Acid Battery State-of-Charge and State-of-Health Research", *Int. J. Smart Grid Clean Energy*, pp. 41-55, 2016.
[8] R. Bindu and S. Thale, "Power Management Strategy for an Electric Vehicle Driven by Hybrid Energy Storage System", *IETE J. Res.*, vol. 68, no. 4, pp. 2801-2811, 2022.
[9] C. C. Hua and M. Y. Lin, "A Study of Charging Control of Lead-Acid Battery for Electric Vehicles", *IEEE Int. Symp. Ind. Electron.*, vol. 1, pp. 135-140, 2000.
[10] R. Li, W. Li, A. Singh, D. Ren, Z. Hou and M. Ouyang, "Effect of External Pressure and Internal Stress on Battery Performance and Lifespan", *Energy Storage Mater.*, vol. 52, pp. 395-429, 2022.
[11] K. Zhang, L. Jiang, Z. Deng, Y. Xie, J. Couture, X. Lin and X. Hu, "An Early Soft Internal Short-Circuit Fault Diagnosis Method for Lithium-Ion Battery Packs in Electric Vehicles", *IEEE/ASME Trans. Mechatronics*, vol. 28, no. 2, pp. 644-655, 2023.
[12] M. A. Fatullah, A. Rahardjo and F. Husnayain, "Analysis of Discharge Rate and Ambient Temperature Effects on Lead Acid Battery Capacity", In Proceedings of the 2019 IEEE International Conference on Innovative Research and Development (ICIRD), 2019, pp. 1-5.
[13] J. M. Bhatt, "Experimental Study About Effect of Temperature on Performance Parameters of Valve Regulated Lead Acid (VRLA) Battery" In Proceedings of the 2019 IEEE International Conference on Sustainable Energy Technologies and Systems (ICSETS), 2019, pp. 285-291.
[14] M. U. Hassan, S. Saha, M. E. Haque, S. Islam, A. Mahmud and N. Mendis, "A Comprehensive Review of Battery State of Charge Estimation Techniques", *Sustain. Energy Technol. Assess.*, vol. 54, p. 102801, 2022.
[15] S. Haldar, S. Mondal, A. Mondal and R. Banerjee, "Battery Management System Using State of Charge Estimation: An IoT Based Approach", In Proceedings of the 2020 National Conference on Emerging Trends on Sustainable Technology and Engineering Applications (NCETSTEA), 2020, pp. 1-5.
[16] M. S. H. Lipu, A. A. Mamun, S. Ansari, M. S. Miah, K. Hasan, S. T. Meraj and N. M. Tan, "Battery Management, Key Technologies, Methods, Issues, and Future Trends of Electric Vehicles: A Pathway Toward Achieving Sustainable Development Goals," *Batteries*, vol. 8, no. 9, p. 119, 2022.
[17] S. Jiang and Z. Song, "A Review on the State of Health Estimation Methods of Lead-Acid Batteries", *J. Power Sources*, vol. 517, p. 230710, 2022.
[18] R. Xiong, L. Li and J. Tian, "Towards a Smarter Battery Management System: A Critical Review on Battery State of Health Monitoring Methods", *J. Power Sources*, vol. 405, pp. 18-29, 2018.
[19] S. Jafari and Y. C. Byun, "Optimizing Battery RUL Prediction of Lithium-Ion Batteries Based on Harris Hawk Optimization Approach Using Random Forest and LightGBM", *IEEE Access*, vol. 11, pp. 87034-87046, 2023.
[20] J. C. Sekhar, B. Domathoti and E. D. Santibanez Gonzalez, "Prediction of Battery Remaining Useful Life Using Machine Learning Algorithms", *Sustainability*, vol. 15, no. 21, p. 15283, 2023.
[21] L. Ma, J. Tian, T. Zhang, Q. Guo and C. Hu, "Accurate and Efficient Remaining Useful Life Prediction of Batteries Enabled by Physics-Informed Machine Learning", *J. Energy Chem.*, vol. 91, pp. 512-521, 2024.
[22] Y. Shen and Y. Ge, "Prediction of State of Charge for Lead-Acid Battery Based on LSTM-Attention and LightGBM", *J. Comput. Inf. Sci. Eng.*, vol. 24, no. 9, p. 090903, 2024.
[23] S. Haldar, S. Mondal, A. Mondal and R. Banerjee, "State of Health and Life Cycle Prediction of In-Vehicle Lead Acid Battery", In Proceedings of the 2022 International Interdisciplinary Conference on Mathematics, Engineering and Science (MESIICON), 2022, pp. 1-6.
[24] M. F. Ge, Y. Liu, X. Jiang and J. Liu, "A Review on State of Health Estimations and Remaining Useful Life Prognostics of Lithium-Ion Batteries", *Measurement*, vol. 174, p. 109057, 2021.
[25] P. Venugopal, S. S. Shankar, C. P. Jebakumar, R. Agarwal, H. H. Alhelou, S. S. Reka and M. E. H. Golshan, "Analysis of Optimal Machine Learning Approach for Battery Life Estimation of Li-Ion Cell", *IEEE Access*, vol. 9, pp. 159616-159626, 2021.
[26] D. Zhou, Z. Li, J. Zhu, H. Zhang and L. Hou, "State of Health Monitoring and Remaining Useful Life Prediction of Lithium-Ion Batteries Based on Temporal Convolutional Network", *IEEE Access*, vol. 8, pp. 53307-53320, 2020.
[27] M. Grunt, S. Pecolt, A. Błażejewski, T. Królikowski and K. Kawa, "Innovative Controller and Remote Battery Capacity Measurement System", *Procedia Comput. Sci.*, vol. 246, pp. 4336-4346, 2024.
[28] Y. Zeng, D. Chalise, S. D. Lubner, S. Kaur and R. S. Prasher, "A Review of Thermal Physics and Management Inside Lithium-Ion Batteries for High Energy Density and Fast Charging", *Energy Storage Mater.*, vol. 41, pp. 264-288, 2021.
[29] S. Barcellona, S. Colnago, G. Dotelli, S. Latorrata and L. Piegari, "Aging Effect on the Variation of Li-Ion Battery Resistance As Function of Temperature and State of Charge", *J. Energy Storage*, vol. 50, p. 104658, 2022.

[30] İ. Aydın and Ö. Üstün, "A Basic Battery Management System Design With IoT Feature for $LiFePO_4$ Batteries", In Proceedings of the 10th International Conference on Electrical and Electronics Engineering (ELECO), 2017, pp. 1309-1313.
[31] V. Gupta, N. Sharma, D. Maram and H. Priyadarshi, "IoT Enabled Data Acquisition System for Electric Vehicle", In Proceedings of the AIP Conference, vol. 2294, no. 1, p. 040002, 2020.
[32] M. S. Gayathri, A. N. Ravishankar, S. Kumaravel and S. Ashok, "Battery Condition Prognostic System Using IoT in Smart Microgrids", In Proceedings of the 3rd International Conference on Internet of Things: Smart Innovation and Usages (IoT-SIU), 2018, pp. 1-6.
[33] J. K. Thomas, H. R. Crasta, K. Kausthubha, C. Gowda and A. Rao, "Battery Monitoring System Using Machine Learning", *J. Energy Storage*, vol. 40, p. 102741, 2021.
[34] A. Rauniyar, M. Irfan, O. D. Saputra, J. W. Kim, A. R. Lee, J. M. Jang and S. Y. Shin, "Design and Development of a Real-Time Monitoring System for Multiple Lead–Acid Batteries Based on Internet of Things", *Future Internet*, vol. 9, no. 3, p. 28, 2017.
[35] G. Krishna, R. Singh, A. Gehlot and S. V. Akram, "An IoT-Based Predictive Model for Improved Battery Management System Using Advanced LSTM Model", *J. Energy Storage*, vol. 101, p. 113694, 2024.
[36] S. Haldar, S. Gol, A. Mondal and R. Banerjee, "IoT-Enabled Advanced Monitoring System for Tubular Batteries: Enhancing Efficiency and Reliability", *E-Prime–Adv. Electr. Eng., Electron. Energy*, vol. 9, p. 100709, 2024.
[37] M. Svendsen, M. Winther-Jensen, A. B. Pedersen, P. B. Andersen and T. M. Sørensen, "Electric Vehicle Data Acquisition System", In Proceedings of the IEEE International Electric Vehicle Conference (IEVC), 2014, pp. 1-7.
[38] S. Echavarría, R. Mejía-Gutiérrez and A. Montoya, "Development of an IoT Platform for Monitoring Electric Vehicle Behaviour", In Proceedings of the Workshop on Engineering Applications, Cham: Springer International Publishing, 2020, pp. 363-374.
[39] G. Pozzato, A. Allam, L. Pulvirenti, G. A. Negoita, W. A. Paxton and S. Onori, "Analysis and Key Findings From Real-World Electric Vehicle Field Data", *Joule*, vol. 7, no. 9, pp. 2035-2053, 2023.